Applied Catalysis B: Environmental 183 (2016) 417–425

Contents lists available at ScienceDirect

Applied Catalysis B: Environmental

journal homepage: www.elsevier.com/locate/apcatb

Dramatic coupling of visible light with ozone on honeycomb-like porous g-C_3N_4 towards superior oxidation of water pollutants

Jiadong Xiao[a,b], Yongbing Xie[a,*], Faheem Nawaz[a,b], Yuxian Wang[a], Penghui Du[a,b], Hongbin Cao[a,c,**]

[a] National Engineering Laboratory for Hydrometallurgical Cleaner Production Technology, Beijing Engineering Research Center of Process Pollution Control, Key Laboratory of Green Process and Engineering, Institute of Process Engineering, Chinese Academy of Sciences, Beijing 100190, China
[b] University of Chinese Academy of Sciences, Beijing 100049, China
[c] Collaborative Innovation Center of Chemical Science and Engineering (Tianjin), Tianjin 300072, China

ARTICLE INFO

Article history:
Received 3 October 2015
Received in revised form 3 November 2015
Accepted 9 November 2015
Available online 14 November 2015

Keywords:
Porous g-C_3N_4
Photocatalytic ozonation
Intermediates
Mechanism
Water treatment

ABSTRACT

Porous g-C_3N_4 (PGCN) has attracted enormous attention due to its accessible nanoporous framework benefiting photocatalytic reactions. Here, we reported a one-pot template-free method to fabricate honeycomb-like PGCN by simply mixing ammonia chloride with the precursor of g-C_3N_4 before calcination. The resulting PGCN exhibited obviously improved photocatalytic activity for *p*-hydroxybenzoic acid (PHBA) degradation under visible light due to its high surface area and enlarged band gap, but PHBA can hardly be mineralized in this process. Hence, for the first time, Vis/PGCN was coupled with ozone in this paper and the results showed that PGCN could trigger a vigorous synergy between photocatalysis and ozonation. Vis/O_3/PGCN led to almost complete mineralization of PHBA with an ozone dosage of 1.5 mg/min, and the process could be further accelerated by increasing the ozone dosage. Such a remarkable mineralization enhancement was mainly attributed to the systematically promoted generation of non-selective hydroxyl radicals (•OH). The high CB level of PGCN benefited electron capture by ozone molecules, thus significantly enhanced charge separation and the decay of ozone into abundant •OH. •OH could vigorously react with PHBA and its ozone-recalcitrant intermediates such as the identified carboxylic acids, finally leading to thorough mineralization. Electrospray ionization–mass spectrometry was adopted to detect the evolution of degradation intermediates in ozonation and Vis/O_3/PGCN, and the mineralization procedure from the original PHBA to CO_2 and H_2O was comprehensively proposed. This study contributes to the integration of sunlight/PGCN with ozone as an efficient metal-free advanced oxidation process for water treatment.

1. Introduction

The utilization of solar energy based on semiconductor photocatalysts for the conversion of pollutants into CO_2 and H_2O is one of the best solutions to solve environmental problems [1]. To date, various visible-light responsive materials, including TiO_2 [2], Ag_3PO_4 [3], $BiVO_4$ [4], CdS [5], Bi_2WO_6 [6], Ag@AgCl [7], C_{60} [8] and graphitic carbon nitride (g-C_3N_4) [9–11] have been developed and their photocatalytic performance for water decontamination has been investigated. Among them, metal-free g-C_3N_4 has drawn worldwide concern for its naturally narrow bandgap of 2.7 eV, permitting it to directly absorb visible light to drive chemical reactions [12]. g-C_3N_4 can be easily obtained through direct polymerization of cheap feedstocks and possesses high thermal and chemical stability due to its tri-s-triazine ring structure [12,13]. Nevertheless, pristine bulk g-C_3N_4 exhibits low photocatalytic efficiency owing to its low surface area and high recombination rate of photogenerated electrons and holes. Nearly 90% of charge carriers can rapidly recombine within 10 ns [14], which remarkably limits the photocatalytic activity of bulk g-C_3N_4. Hence, it is highly necessary to increase the active surface area of g-C_3N_4 and to promote the separation of charge carriers during photocatalytic reactions.

Enormous efforts have been devoted to improving the photocatalytic activity of g-C_3N_4, typically including doping with nonmetallic elements [15,16], deposition with metal atoms [17,18], compositing with other semiconductors [19,20] or conjugated

* Corresponding author. Fax: +86 01082544844.
** Corresponding author at: National Engineering Laboratory for Hydrometallurgical Cleaner Production Technology, Beijing Engineering Research Center of Process Pollution Control, Key Laboratory of Green Process and Engineering, Institute of Process Engineering, Chinese Academy of Sciences, Beijing 100190, China.
E-mail addresses: ybxie@ipe.ac.cn, beyondxyb@hotmail.com (Y. Xie), hbcao@ipe.ac.cn (H. Cao).

http://dx.doi.org/10.1016/j.apcatb.2015.11.010
0926-3373/

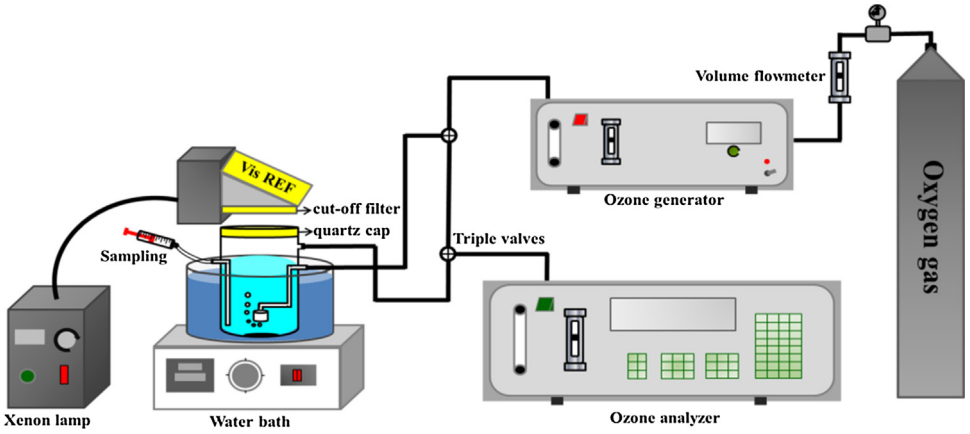

Scheme 1. Experimental setup of photocatalytic ozonation.

polymers [21,22] and nanostructure engineering [10,23–26]. Among them, porous g-C_3N_4 (PGCN) is especially attractive due to its accessible porous framework with a large surface area. PGCN features facilitated mass transfer ability, enhanced light harvesting property and improved separation and migration efficiency of charge carriers owing to its nanoporous structure [10,25,26]. Generally, PGCN can be obtained via a soft-templating or silica-templating method [26–28]. However, for soft template synthesis, some carbon is still residual from the templating polymers in the final product, which might reduce its catalytic activity [27]. The silica-templating synthesis involves further removal of the silica by aqueous ammonia or hydrogen fluoride [26,28], which is hazardous and inconvenient. To develop a facile synthetic method of PGCN remains a significant issue.

On the other hand, integrating photocatalysis with other advanced oxidation processes (AOPs) can be another solution to promote the separation and migration of charge carriers during photocatalytic reactions [29]. In this sense, coupling g-C_3N_4 photocatalysis with ozone can be a promising treatment approach. Since ozone is a more powerful oxidant than oxygen, it can quickly capture photoinduced electrons during photochemical reactions. This would promote the separation of charge carriers and decomposition of ozone, and consequently generate more oxidative species to expedite the degradation and mineralization of water pollutants [29–32]. TiO_2 was the most widely applied in photocatalytic ozonation [29], indicating a quite limited optional scope. Till very recently, three studies announced that bulk g-C_3N_4 could trigger a super synergy between visible-light photocatalysis and ozonation to enhance the oxidation efficiency [33–35]. However, an intensive investigation is still requisite on the mechanism for the enhanced mineralization of organics from photocatalysis to photocatalytic ozonation using PGCN as catalyst. It is also significant to study the evolution of reactive species and the mineralization pathway of water pollutants in Vis/O_3/PGCN, in order to better understand the oxidation mechanism of this integrated technology.

Herein, we reported a one-pot template-free method to fabricate a series of PGCN (PGCN-1, PGCN-2, PGCN-3 and PGCN-4) and applied in removal of *p*-hydroxybenzoic acid (PHBA). PHBA was chosen as the targeted pollutant for it is very commonly found in a great variety of agroindustrial wastewaters and especially toxic and refractory to anaerobic biological treatment [36,37]. Comparing with bulk g-C_3N_4, PGCN-3 exhibited greatly improved photocatalytic activity for *p*-hydroxybenzoic acid (PHBA) degradation mainly due to its high surface area and enlarged band gap, while the final PHBA mineralization rate was nearly zero. The integration of PGCN-3 photocatalysis and ozoantion lead to almost complete mineralization of PHBA, and the mineralization could be further accelerated by increasing the ozone dosage. Trapping experiments were conducted to determine the evolution of reactive species from Vis/PGCN-3 to Vis/O_3/PGCN-3. Electrospray ionization–mass spectrometry (ESI–MS) was further adopted to detect the evolution of degradation intermediates both in ozonation and Vis/O_3/PGCN-3. Among the identified by-products, carboxylic acids were found to be highly recalcitrant to ozonation, while they could be rapidly eliminated by large amounts of non-selective $^{\bullet}$OH in Vis/O_3/PGCN-3. Meanwhile, the complete mineralization process from the original PHBA to CO_2 and H_2O was uncovered.

2. Experimental

2.1. Materials and reagents

Thiourea, ammonium chloride (NH_4Cl), PHBA and oxalic acid (OA) were purchased from Sinopharm Chemical Reagent Co., Ltd., China. *Tert*-butanol (tBA), *p*-benzoquinone (pBQ) and ammonium oxalate (AO) were supplied by Xilong Chemical Co., Ltd., China. Sodium azide (NaN_3) was purchased from Tianjin Fuchen Chemical Reagents factory, China. Ultrapure oxygen (purity 99.999%) and nitrogen gas (purity 99.999%) were provided by Beijing Qianxi Gas Co., Ltd., China. All chemicals used in this study were at least in analytical grade without further purification. Ultra-pure water was used for all synthesis and treatment.

2.2. Preparation of PGCN

PGCN was prepared by pyrolysis of a mixture of thiourea and NH_4Cl in air atmosphere. Typically, 10 g of thiourea and a certain amount of NH_4Cl (2, 5, 10 or 15 g) were added into 10 mL ultrapure water in a 100 mL beaker. The beaker was then placed in a water bath with stirring at 65 °C for a few min. After natural dying in ambient condition, the white solid was transferred into an alumina crucible. The crucible was then put in a muffle furnace and heated to 550 °C with a rate of 15 °C/min and maintained for 4 h. The final products were collected, washed with ultrapure water and ethanol, and dried in an oven at 60 °C for 12 h. The samples prepared with 2, 5, 10 and 15 g of NH_4Cl were labeled as PGCN-1, PGCN-2, PGCN-3 and PGCN-4, respectively.

2.3. Catalyst characterization

The crystal phase was characterized by X-ray Diffraction (XRD) (X' PERT-PRO MPD) with a $Cu_{K\alpha}$ irradiation ($\lambda = 0.15406$ nm). The morphologies and structures of the prepared samples were further investigated by field-emission transmission electron microscopy (FETEM, JEM-2100F, JEOL, Japan). The Brunauer–Emmett–Teller (BET) surface areas were measured by an automated gas sorption

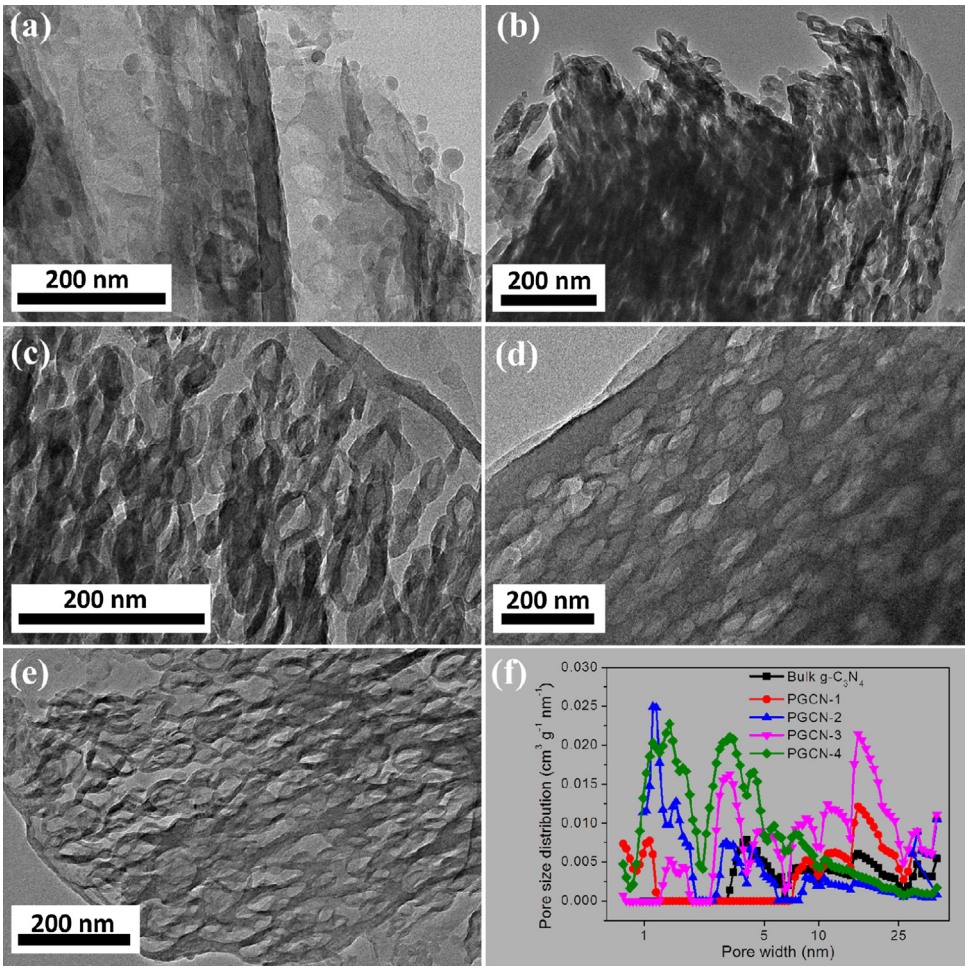

Fig. 1. FETEM images of bulk g-C_3N_4 (a), PGCN-1 (b), PGCN-2 (c), PGCN-3 (d) and PGCN-4 (e); pore size distribution of the prepared materials (f).

analyzer (Autosorb-iQ, Quantachrome, USA). Pore size distribution was calculated with the non-localized density functional theory method using adsorption data. The UV–vis diffuse reflectance spectra (DRS) of the samples were obtained using Varian Cary 5000, USA. X-ray photoelectron spectroscopy (XPS) data were obtained on an ESCALAB 250Xi instrument (Thermo Fisher Scientific, USA).

2.4. Photocatalysis, ozonation and photocatalytic ozonation experiments

As shown in Scheme 1, the photocatalytic ozonation was carried out at 25 °C under visible light (420–800 nm) in a 500 mL cylindrical borosilicate glass reactor with a quartz cap and a porous glass plate at the bottom, containing 400 mL solution with 20 mg/L of PHBA and 0.5 g/L of catalyst. Typically, the gaseous ozone was continuously bubbled through the porous plate into the reactor with a flow rate of 100 mL/min and various concentrations (15, 40 and 65 mg/L). Meanwhile, the solution was irradiated under visible light (420–800 nm) with an average radiant flux of 360 mW/cm^2. Ozone was generated from ultrapure oxygen by an ozone generator (Anseros COM-AD-01, Germany). Visible light was provided by a 300 W Xenon lamp (CEL-NP2000, Aulight Co., Ltd., China) with a visible-light reflector and a 420 nm cutoff filter. Single photocatalysis and ozonation experiments were conducted using the same reactor. For photocatalytic degradation, during each run, the solution was magnetically stirring in dark for 30 min to obtain an adsorption-desorption equilibrium before reaction.

2.5. Analytical methods

The concentrations of PHBA and OA were analyzed by high performance liquid chromatography (HPLC, Agilent series 1200, USA) equipped with a Zorbax SB-Aq column and a UV–vis detector qualified at 240 nm and 210 nm, respectively. The mobile phase was a mixture of methanol and water containing 10 mM H_3PO_4 (20/80%, v/v). Total organic carbon (TOC) was determined with a TOC-VCPH analyzer (Shimadzu, Japan). The electron spin resonance (ESR) signals of radicals spin trapped by 5,5-dimethyl-1-pyrroline (DMPO) were detected at ambient temperature on a JEOL (JES-FA200) spectrometer. The degradation intermediates were determined by ESI–MS (micrOTOF-Q, Bruker, Germany). The ESI interface was operated in negative mode, and the parameters were set as follows: capillary voltage at 4500 V; nebulizer gas (N_2) pressure at 0.4 bar; dry heater temperature at 180 °C; dry gas (N_2) flow rate at 4.0 L/min. Full-scan spectra were obtained by m/z scanning from 21 to 800. All the ozone-involved samples were promptly pre-purged by ultrapure N_2 to remove the residual dissolved ozone before analysis.

3. Results and discussion

3.1. Structural and optical properties of PGCN

The PGCN materials were prepared by thermal condensation of mixed thiourea and NH_4Cl in air atmosphere. By adjusting the mass ratio of NH_4Cl to thiourea, the porous structure of g-C_3N_4 could be

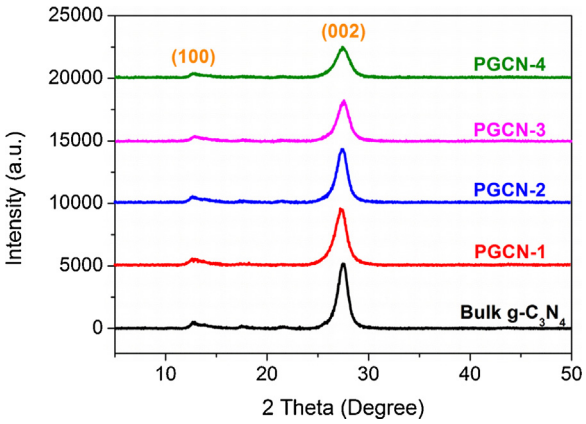

Fig. 2. XRD patterns of bulk g-C_3N_4, PGCN-1, PGCN-2, PGCN-3 and PGCN-4.

effectively controlled. Fig. 1a–e shows the FETEM images of bulk g-C_3N_4, PGCN-1, PGCN-2, PGCN-3 and PGCN-4, respectively. The bulk g-C_3N_4 exhibited a typically bulk morphology with dense and thick nanosheets. With the addition of NH_4Cl in the precursor, loose layers and abundant nanopores were gradually formed. PGCN-1, PGCN-2, PGCN-3 and PGCN-4 displayed loose and honeycomb-like nanoarchitectures. The pore size distribution curves in Fig. 1f further confirmed the nanoporous structure of PGCN. Generally, the overall number of nanopores increased with addition amount of NH_4Cl in the precursor, while the pore sizes of PGCN cannot be accurately controlled by the addition amount of NH_4Cl. Bulk g-C_3N_4 had few pores, while PGCN-1 possessed a relatively larger amount of micropores (1.0 nm) and mesopores (8.5, 11.2, 16.0 and 30.1 nm). PGCN-2 had abundant micropores (1.1 nm) and less mesopores. Small mesopores (2.9 nm) and large mesopores (8.5, 11.2 and 16.0 nm) could be observed in PGCN-3. Best of all, PGCN-4 possessed both abundant micropores (1.4 nm) and small mesopores (3.0, 4.2, 5.7 and 7.5 nm). Correspondingly, PGCN-4 had the highest specific surface area (112.0 m^2/g), which was 5.2 times as high as that of bulk g-C_3N_4. The surface areas of PGCN-1, PGCN-2 and PGCN-3 were 42.5, 46.7 and 83.5 m^2/g, respectively.

NH_4Cl as a bubbling template influenced the polymerization of thiourea from two aspects. One was the decreased polymerization degree of g-C_3N_4. Fig. 2 presents the XRD patterns of the prepared materials, and a typical graphitic stacking C_3N_4 structure was confirmed by two obvious peaks at 13.0° and 27.4°, respectively [9]. The peak intensities of PGCN were lower than those of bulk g-C_3N_4, indicating a less condensation degree and crystallinity of g-C_3N_4. The XRD peaks at 27.4° of PGCN were broader than that of bulk g-C_3N_4, which was attributed to the delamination of the thick bulk g-C_3N_4 into thin nanosheets with several atomic layers [38].This was also in accordance with the thin and porous morphology of PGCN samples. The other was that the burst of bubbles from NH_4Cl thermolysis would result in a large number of nanopores in the final g-C_3N_4. Gas bubbles, which generated during the process of g-C_3N_4 condensation, played a significant role for the generation of porous structure [10,25]. The thermolysis of NH_4Cl could release gaseous NH_3 and HCl during the polymerization of thiourea. Large amounts of soft bubbles were thereby generated and later burst, leading to the formation of abundant pores in the layers.

The XPS measurement was conducted to determine the chemical state of PGCN-3, as shown in Fig. 3. Signals of C, N and O elements were found in the spectra survey (Fig. 3a), and no peaks assigned to S or Cl species could be detected (Fig. 3e and f). This implied that sulfur in thiourea and chlorine in NH_4Cl were completely released into air during the heating process. The C1s spectra in Fig. 3b showed three main peaks, which could be assigned to adventitious carbon species (284.8 eV), C—$(N)_3$ (286.1 eV) and N—C=N (288.0 eV), respectively [39]. The high-resolution N1s spectra could be fitted into four peaks centered at about 398.4, 399.0, 400.6 and 404.2 eV, respectively (Fig. 3c) [39,40]. The main signals showed the occurrence of the sp^2-bonded N involved in the triazine rings (C—N=C, 398.4 eV) and tertiary nitrogen groups (N—$(C)_3$, 399.0 eV). The weak peak at 400.6 eV indicated the presence of amino functional groups (C—N—H), originating from the defective condensation of heptazine substructures. The very weak peak at 404.2 eV was attributed to the charging effects or positive charge localization in the heterocycles. There were three main signals in O1s spectra, which could be assigned to the hydroxyl groups (—OH, 531.7 eV), O—C—N (532.3 eV) and chemisorbed H_2O (533.4 eV), respectively [39]. The contained oxygen (O—C—N) in the samples presumably came from the heating treatment in the presence of air. The surface C/N atomic ratio of PGCN-3 was 1.29 in a semi-quantitative fashion. It indicated that PGCN-3 were carbon-rich and nitrogen-poor in terms of the nominal theoretical value of 0.75 for g-C_3N_4.

The optical properties of the prepared samples were examined by UV–vis DRS, as displayed in Fig. 4. The PGCN samples showed slightly reduced absorption than bulk g-C_3N_4 especially in the region of 420–550 nm, while PGCN-4 exhibited enhanced absorption in the range of 600–800 nm. The bandgaps were determined correspondingly (Fig. 4b). The bandgaps (Eg), which were estimated from the intercept of the tangents to the plots of $(\alpha h\upsilon)^2$ versus $h\upsilon$ (Fig. 4b), were 2.78, 2.86, 2.86, 2.85 and 2.88 eV for bulk g-C_3N_4, PGCN-1, PGCN-2, PGCN-3 and PGCN-4, respectively. The PGCN samples had almost equal Eg values, which were ~0.1 eV higher than that of bulk g-C_3N_4. This was in agreement with the reported literature [25]. The additionally released NH_3 (g) and HCl (g) would weaken the condensation process and reduce the degree of π-conjugated polymeric network, resulting in an increase of bandgap [25]. The enlarged band gap could increase the redox capability of electrons and holes and enhanced photocatalytic activity of g-C_3N_4.

3.2. Enhanced photocatalytic activity of PGCN

The photocatalytic activities of the materials were evaluated by PHBA degradation under visible light, as shown in Fig. 5. The photocatalytic degradation generally followed pseudo-zero-order kinetics according to the linear trends of C/C_0 versus the irradiation time. The apparent rate constants were calculated correspondingly, as presented in Fig. 5b. It was obvious that all the PGCN samples demonstrated enhanced photocatalytic activity than bulk g-C_3N_4 for decomposition of PHBA under visible light. When the mass fraction of NH_4Cl to thiourea reached 1.0, the resultant photocatalyst PGCN-3 exhibited the highest photocatalytic performance. However, when further increasing the proportion of NH_4Cl, the photocatalytic performance of PGCN-4 significantly decreased. The specific surface area of PGCN-3 (83.5 m^2/g) was 25.4% lower than that of PGCN-4 (112.0 m^2/g), while the triggered PHBA removal rate constant (5.84×10^{-2} mg/L min) was 39.0% higher than that of PGCN-4 (4.20×10^{-2} mg/L min). Generally, high surface area can lead to enhanced adsorption and diffusion of reactants and products. However, it may also introduce more surface defects that could capture charge carriers and hinder their involvement in the photocatalytic reaction [25,41]. The superior activity of PGCN-3 to PGCN-4 was presumably attributed to a less amount of surface defects and higher crystallinity.

A series of trapping experiments were adopted using tBA [42], pBQ [42], NaN_3 [43] and AO [42] as the scavenger of •OH, superoxide radicals ($^{\bullet}O_2^-$), singlet oxygen ($^1O_2$) and positive holes (h^+), respectively, in order to determine the involved reactive species during photocatalytic degradation of PHBA. Fig. 6 shows PHBA removal in the presence of various scavengers. The addition of tBA made a negligible difference on the degradation of PHBA, while

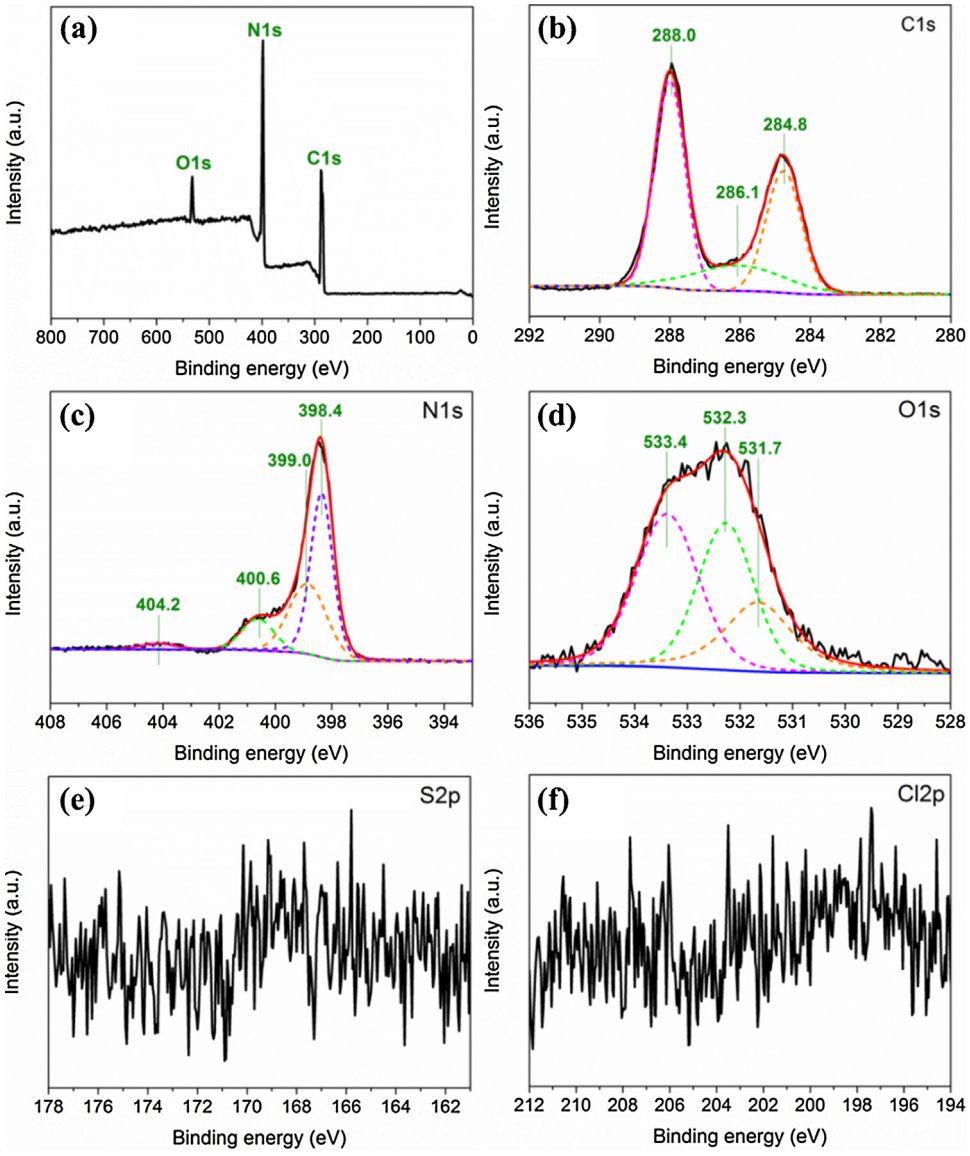

Fig. 3. XPS spectra of PGCN-3 including the survey (a), C1s (b), N1s (c), O1s (d), S2p (e) and Cl2p (f).

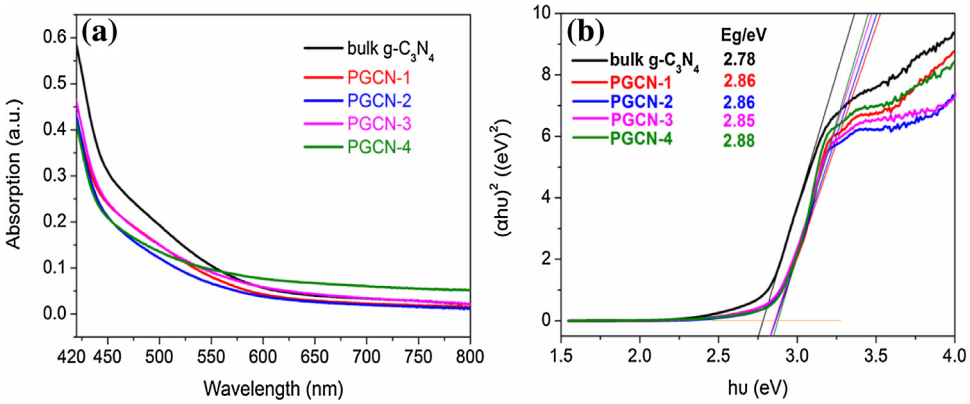

Fig. 4. UV–vis DRS spectra (a) and the bandgaps (b) of bulk g-C_3N_4, PGCN-1, PGCN-2, PGCN-3 and PGCN-4.

pBQ slightly suppressed PHBA removal. It indicated that •OH was not involved in the photocatalytic reactions, and $^{\bullet}O_2^-$ only played a small part. NaN_3 and AO could both moderately inhibit PHBA removal during photocatalysis. The photocatalytic degradation was mainly attributed to the direct reaction of PHBA with $^1O_2$ and h^+.

3.3. Enhanced PHBA mineralization by photocatalytic ozonation

Fig. 7 shows the TOC removal in mineralizing PHBA by Vis/PGCN-3, single ozonation and Vis/O_3/PGCN-3, respectively. Although 17.9% of PHBA was removed in Vis/PGCN-3 at 60 min

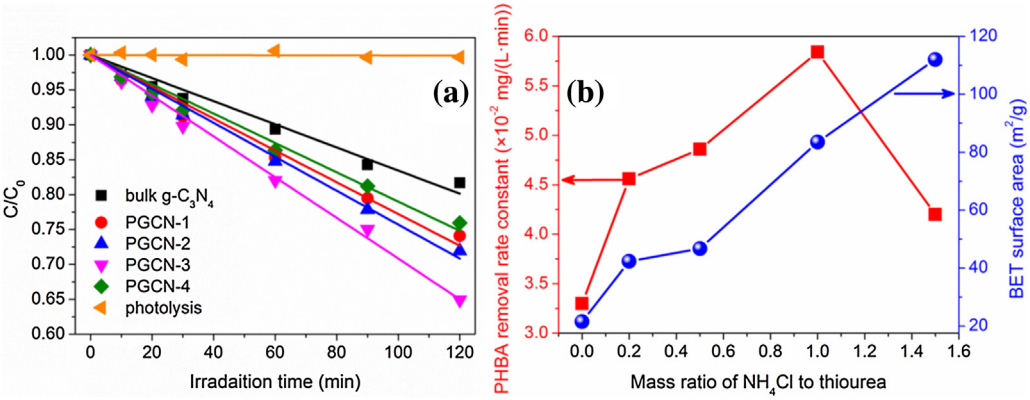

Fig. 5. (a) Photocatalytic degradation of PHBA with various catalysts; (b) BET surface areas and PHBA photocatalytic removal rate constant of PGCN fabricated with different mass ratio of NH_4Cl to thiourea as the precursor.

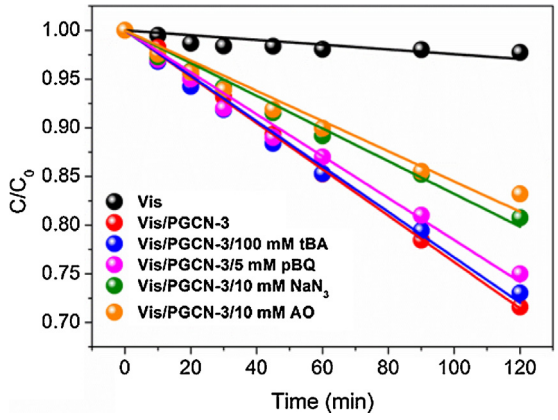

Fig. 6. Photocatalytic degradation of PHBA in the presence of various scavengers.

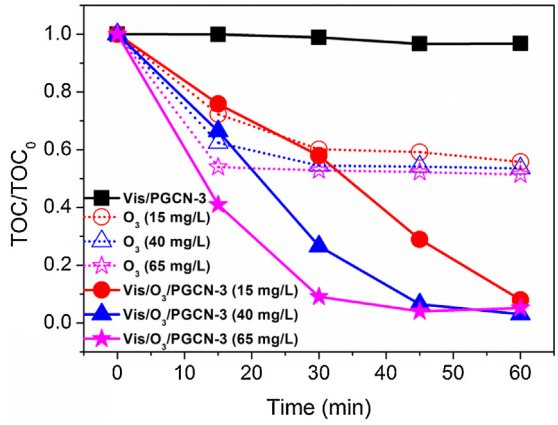

Fig. 7. TOC removal in treating PHBA by Vis/PGCN-3, O_3 and Vis/O_3/PGCN-3 with an ozone concentration at 15, 40 and 65 mg/L (gas flow rate: 100 mL/min; light intensity: 360 mW/cm^2; solution volume: 400 mL; PHBA concentration: 20 mg/L; catalyst dosage: 0.5 g/L).

(Fig. 5a), the TOC removal rate was only 3.3%. It meant that 17.9% of PHBA reacted with $^1O_2$ or h^+ during photocatalysis to form stable intermediates which were highly refractory to further mineralization. Compared to photocatalysis, ozonation exhibited moderately enhanced mineralization of PHBA. TOC was rapidly removed during the first 15 min in single ozonation, while the removal rate of TOC turned slower within the second 15 min. Nearly no TOC was eliminated from 30 to 60 min. This phenomenon was more obvious when improving the ozone concentration from 15 mg/L to 60 mg/L. Enhancing ozone dosage could accelerate PHBA mineralization in the first 15 min, while the final TOC removal was still quite limited. The final TOC removal was 44.2%, 46.5% and 48.6% in ozonation with an ozone concentration of 15, 40 and 65 mg/L, respectively. More importantly, PHBA mineralization was dramatically facilitated when coupling Vis/PGCN-3 with ozonation. The final TOC removal was 92.0%, 97.0% and 95.0% in Vis/O_3/PGCN-3 with an ozone concentration of 15, 40 and 65 mg/L, which was 44.5%, 47.2% and 43.1% higher than the sum of that in Vis/PGCN-3 and ozonation, respectively. It indicated that PGCN-3 could trigger a vigorous synergy between photocatalysis and ozonation for efficient mineralization of water pollutants. It was also found that a higher ozone dosage would greatly expedite the mineralization of PHBA into carbon dioxide and water in Vis/O_3/PGCN-3.

In addition, the TOC removal in O_3/PGCN-3 and Vis/O_3 was quite close to that in single ozonation, as shown in Fig. S1. This indicated that PGCN-3 had negligible activity in catalytic ozonation, and no synergistic effect was observed between photolysis and ozonation for PHBA mineralization. This result was in accordance with our previous work [34,35], confirming the key bridging role of PGCN-3 between visible-light irradiation and ozone molecules.

3.4. Mechanism for PHBA mineralization by Vis/O_3/PGCN-3

It is well known that two types of reaction mechanisms contribute to the removal of pollutants in ozone-involved AOPs. These mechanisms usually develop in consecutive stages: during the first minutes ozone reacts very fast with the unsaturated compounds to form less reactive intermediates (direct mechanism); and then these refractory compounds are eliminated by reactive radicals (indirect mechanism) [29,30]. Fig. 8a shows the PHBA removal by Vis/PGCN-3, O_3 and Vis/O_3/PGCN-3 with or without tBA and AO. It could be seen that PHBA reacted rapidly with ozone. The PHBA removal rate by single ozonation was as high as 69.0% within 20 min, while that was only 4.4% in Vis/PGCN-3. Among the three processes, Vis/O_3/PGCN-3 revealed the highest rate of PHBA degradation. PHBA was completed eliminated by Vis/O_3/PGCN-3 in 12.5 min, while 50.4% and 97.0% of PHBA were remaining in ozonation and Vis/PGCN-3, respectively. It indicated that other reactive species were generated and also responsible for PHBA degradation besides direct oxidation of ozone.

As shown in Fig. 8a, the addition of tBA could significantly inhibited PHBA elimination. The PHBA removal rate of Vis/O_3/PGCN-3/tBA was quite close to the sum of that of Vis/PGCN-3 and ozonation. This implied that the synergy between Vis/PGCN-3 and ozonation was dominantly attributed to the promoted generation of •OH. Large amounts of •OH were formed and mainly

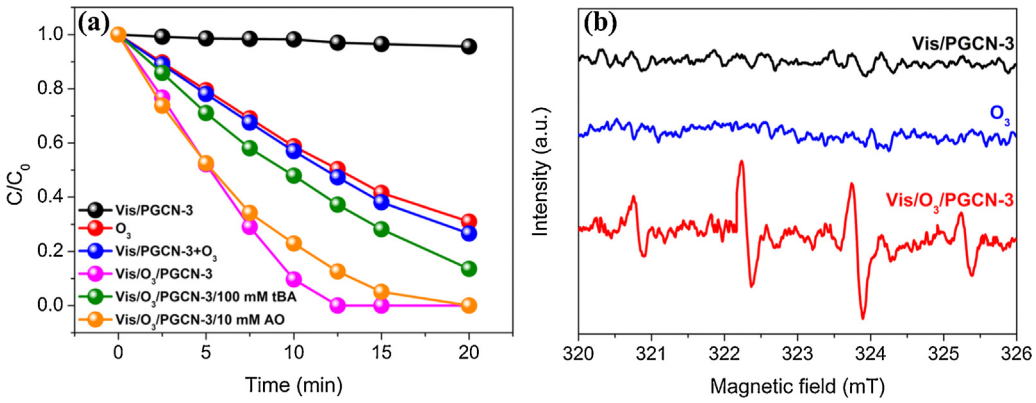

Fig. 8. (a) PHBA removal by various oxidation methods with or without tBA and AO (gas flow rate: 100 mL/min; ozone concentration: 15 mg/L; light intensity: 360 mW/cm^2; solution volume: 400 mL; PHBA concentration: 20 mg/L; catalyst dosage: 0.5 g/L); (b) ESR spectra of DMPO-•OH adducts in Vis/PGCN-3, O_3 and Vis/O_3/PGCN-3 systems.

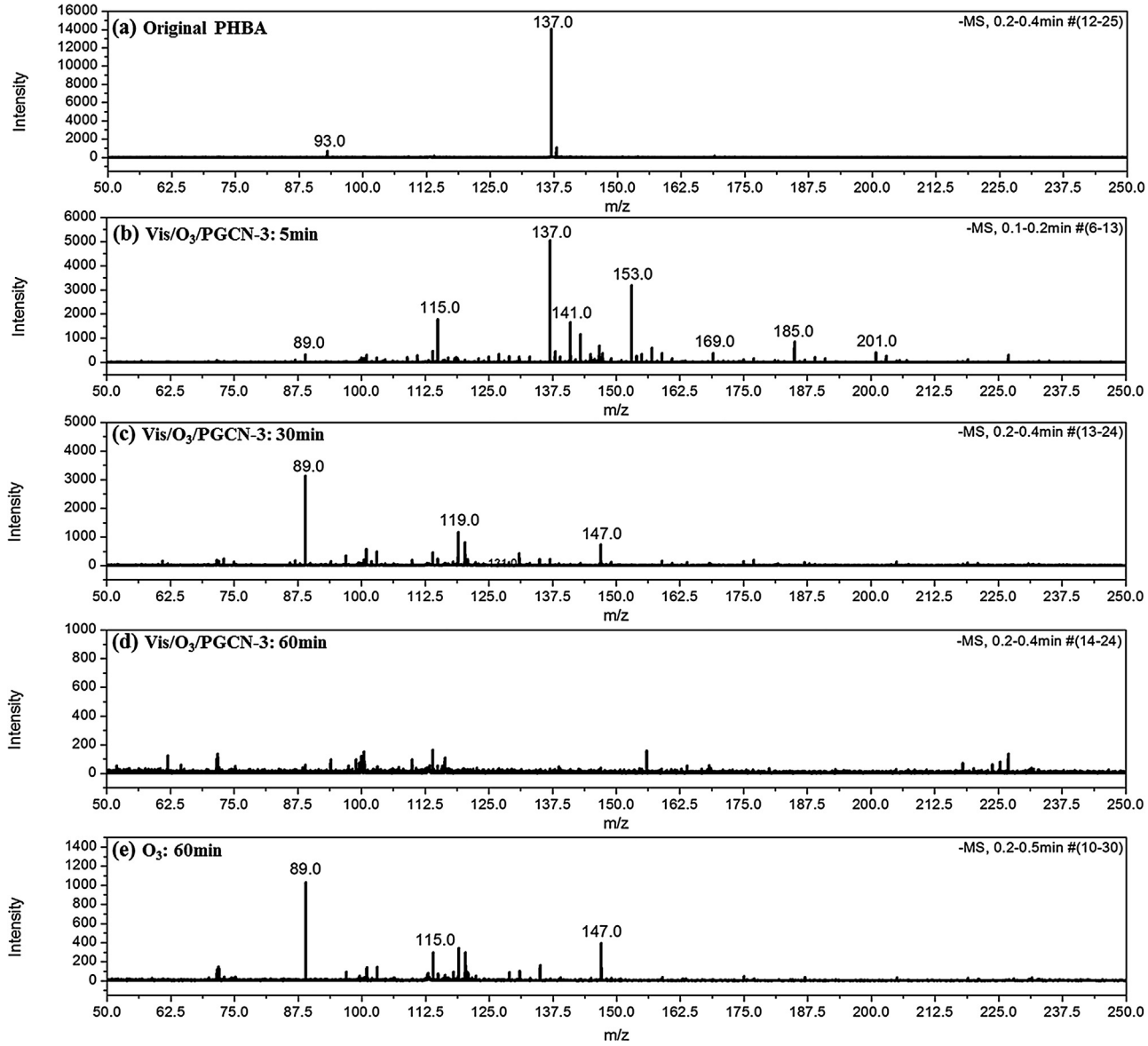

Fig. 9. ESI–MS spectra of initial PHBA (a), intermediates in PHBA mineralization by Vis/O_3/PGCN-3 at 5 min (b), 30 min (c) and 60 min (d), and final products in PHBA mineralization by ozonation at 60 min (e).

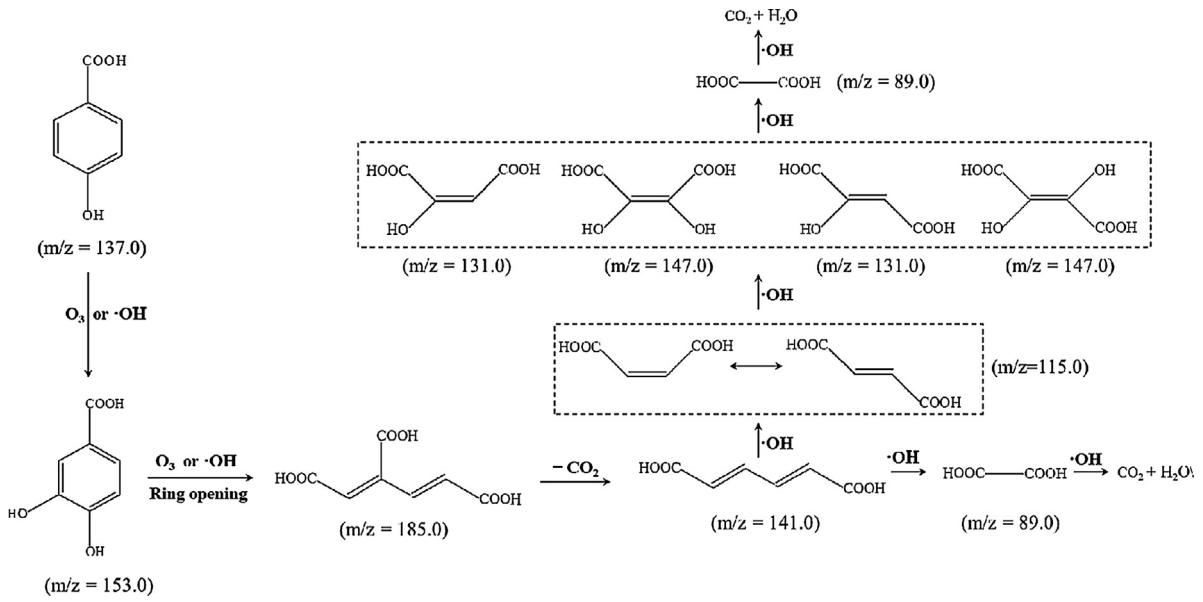

Fig. 10. Proposed mechanism for PHBA mineralization in Vis/O_3/PGCN-3.

accounted for the enhanced mineralization of the original pollutant and refractory intermediates in Vis/O_3/PGCN-3, which was in accordance with the reported UV/O_3/TiO_2 system [30]. The •OH generation was further confirmed by the ESR spectra in Fig. 8b. No signals assigned to •OH were found in Vis/PGCN-3 and single ozonation systems, while that can be conspicuously seen in the integrated Vis/O_3/PGCN-3 process. Additionally, h^+ also played a very small part for PHBA degradation, according to the slight inhibition of AO. During Vis/O_3/PGCN-3, PGCN-3 could absorb the visible-light photons to generate electrons upon conduction band (CB) and holes upon valance band (VB) (Eq. (1)). The CB minimum of g-C_3N_4 was reported to be −1.3 V (versus NHE), while its VB maximum was + 1.40 V (versus NHE) [11–13]. Owing to its more negative CB potential than that of TiO_2 (−0.5 V versus NHE), ozone could quickly capture the strong reducing electrons upon CB of PGCN-3. An ozonide radical ($•O_3^-$) was thus formed (Eq. (2)), and it rapidly reacted with H^+ in the solution to give a $HO_3•$ radical (Eq. (3)), which subsequently decomposed into •OH (Eq. (4)).

$$PGCN - 3 \xrightarrow{Vis} e^- + h^+ \quad (1)$$

$$O_3 + e^- \rightarrow •O_3^- \quad (2)$$

$$•O_3^- + H^+ \rightarrow HO_3• \quad (3)$$

$$HO_3• \rightarrow O_2 + •OH \quad (4)$$

Notably h^+ were incapable to directly oxidize the surface hydroxyl groups or adsorbed water molecules to form •OH, as the VB potential of g-C_3N_4 is less than E^0 ($•OH/OH_{suf}^-$) or E^0 ($•OH/H_2O_{ads}$) [33–35].

The intermediates in PHBA mineralization by Vis/O_3/PGCN-3 and ozonation were further detected through ESI–MS, in order to uncover the reaction pathway and better understand the reason for dramatically enhanced mineralization level of Vis/O_3/PGCN-3. Fig. 9 shows the ESI–MS spectra of initial PHBA, intermediates in Vis/O_3/PGCN-3 at 5 min, 30 min and 60 min, and final products in ozonation at 60 min. Based on this, the major by-products generated during Vis/O_3/PGCN-3 were identified. Fig. 10 illustrates the identified intermediates and PHBA mineralization pathway in Vis/O_3/PGCN-3. In the first stage, both ozone and •OH could electrophilically attack the aromatic ring of PHBA to form protocatechuic acid (m/z = 153.0), which was further oxidized into 1,3-butadiene-1,2,4-tricarboxylic acid (m/z = 185.0) with ring opening. Muconic acid (m/z = 141.0) was quickly formed via decarboxylation of 1,3-butadiene-1,2,4-tricarboxylic acid. Afterwards, the non-selective •OH dominantly accounted for further mineralization of carboxylic acids including muconic acid (m/z = 141.0), maleic/fumaric acid (m/z = 115.0), 2-hydroxyl-maleic/2-hydroxyl-fumaric acid (m/z = 131.0), 2,3-dihydroxyl-maleic/2,3-dihydroxyl-fumaric acid (m/z = 147.0), and finally OA (m/z = 89.0). Further oxidation of OA would produce CO_2 and H_2O, and the mineralization of PHBA was thus completely accomplished.

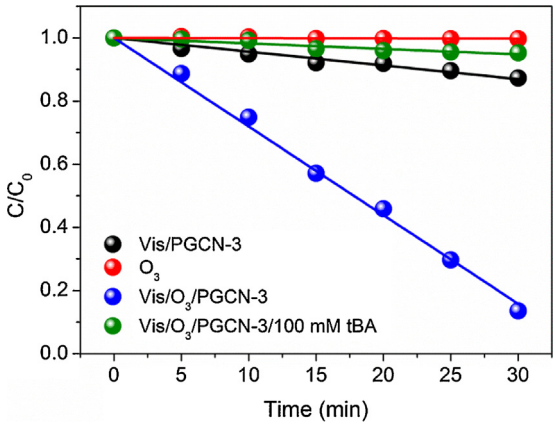

Fig. 11. Comparison of OA removal by Vis/PGCN-3, ozonation and Vis/O_3/PGCN-3 (gas flow rate: 100 mL/min; ozone concentration: 40 mg/L; light intensity: 360 mW/cm^2; solution volume: 400 mL; OA concentration: 1 mM; catalyst dosage: 0.5 g/L).

It was also found that some carboxylic acids such as OA (m/z = 89.0), maleic/fumaric acid (m/z = 115.0) and 2,3-dihydroxyl-maleic/2,3-dihydroxyl-fumaric acid (m/z = 147.0) were remaining in ozonation system according to the corresponding ESI–MS peaks in Fig. 9e. It indicated that these compounds were highly recalcitrant to ozonation, which led to ~55.8% of TOC residual in the solution (Fig. 7). OA, as one of the refractory intermediates, was then chosen as another targeted pollutant to test the oxidation efficiencies of Vis/PGCN-3, ozonation and Vis/O_3/PGCN-3. As shown in Fig. 11, OA was highly stable in ozonation system as no OA was removed by single ozonation. Vis/PGCN-3 led to 13.0% of OA removal within 30 min, while that was 86.5% in

Vis/O_3/PGCN-3. The apparent OA mineralization rate constant in Vis/O_3/PGCN-3 was 2.81×10^{-2} mM/L min, which was 6.5 times as high as the sum of that in Vis/PGCN-3 and ozonation (Table S2). The integrated Vis/O_3/PGCN-3 process exhibited outstanding mineralization of refractory byproducts compared to single photocatalysis and ozonation. The addition of tBA could completely block OA degradation (Fig. 11), reconfirming the dominated role of •OH in mineralizing water pollutants by Vis/O_3/PGCN-3. Hence, a large amount of non-selective •OH were systematically generated triggered by ozone capturing highly reducing electrons (Eqs. (1)–(4)), and could vigorously react with the pollutant and further its recalcitrant intermediates consequently to realize the complete mineralization in Vis/O_3/PGCN-3.

4. Conclusions

We reported a facile one-step template-free method to fabricate honeycomb-like PGCN by mixing NH_4Cl with thiourea as the precursor. The resulting PGCN-3 exhibited obviously improved photocatalytic activity for PHBA degradation mainly due to its high surface area and enlarged band gap. It also strikingly triggered a vigorous synergy between photocatalysis and ozonation for PHBA mineralization. The final TOC removal in Vis/O_3/PGCN-3 was 92.0% with an ozone dosage of 1.5 mg/min, which was 44.5% higher than the sum of that in Vis/PGCN-3 and ozonation. Such a remarkable enhancement was mainly attributed to the systematically promoted generation of non-selective •OH. The high CB level of PGCN-3 benefited electron capture by ozone molecules, thus significantly enhanced charge separation and the decay of ozone into abundant •OH. •OH could vigorously react with PHBA and its recalcitrant intermediates, leading to thorough mineralization in Vis/O_3/PGCN-3. The present work puts forward an efficient metal-free Vis/O_3/g-C_3N_4 method for mineralization of water pollutants, and sheds light on the generation of reactive species as well as the mineralization pathway in this integrated process. It is also expected to advance the fundamental research and application of solar photocatalytic ozonation and other AOPs using sunlight as energy source.

Acknowledgements

The authors greatly appreciate the financial support from the National Natural Science Foundation of China (No. 21207133) and the National Science Fund for Distinguished Young Scholars of China (No. 51425405).

Appendix A. Supplementary data

Supplementary data associated with this article can be found, in the online version, at http://dx.doi.org/10.1016/j.apcatb.2015.11.010.

References

[1] L.M. Sun, L. Xiang, X. Zhao, C.J. Jia, J. Yang, Z. Jin, X.F. Cheng, W.L. Fan, ACS Catal. 5 (2015) 3540–3551.
[2] A. Naldoni, M. Allieta, S. Santangelo, M. Marelli, F. Fabbri, S. Cappelli, C.L. Bianchi, R. Psaro, V.D. Santo, J. Am. Chem. Soc. 134 (2012) 7600–7603.
[3] B. Wang, L. Wang, Z.B. Hao, Y. Luo, Catal. Commun. 58 (2015) 117–121.
[4] M.C. Long, W.M. Cai, J. Cai, B.X. Zhou, X.Y. Chai, Y.H. Wu, J. Phys. Chem. B 110 (2006) 20211–20216.
[5] N. Zhang, M.Q. Yang, Z.R. Tang, Y.J. Xu, J. Catal. 303 (2013) 60–69.
[6] L.S. Zhang, W.Z. Wang, Z.G. Chen, L. Zhou, H.L. Xu, W. Zhu, J. Mater. Chem. 17 (2007) 2526–2532.
[7] P. Wang, B.B. Huang, X.Y. Qin, X.Y. Zhang, Y. Dai, J.Y. Wei, M.H. Whangbo, Angew. Chem. Int. Ed. 47 (2008) 7931–7933.
[8] K.J. Moor, J.H. Kim, Environ. Sci. Technol. 48 (2014) 2785–2791.
[9] X.C. Wang, K. Maeda, A. Thomas, K. Takanabe, G. Xin, J.M. Carlsson, K. Domen, M. Antonietti, Nat. Mater. 8 (2009) 76–80.
[10] M. Zhang, J. Xu, R.L. Zong, Y.F. Zhu, Appl. Catal. B: Environ. 147 (2014) 229–235.
[11] H.Q. Sun, G.L. Zhou, Y.X. Wang, A. Suvorova, S.B. Wang, ACS Appl. Mater. Inter. 6 (2014) 16745–16754.
[12] J.S. Zhang, Y. Chen, X.C. Wang, Energy Environ. Sci. 8 (2015) 3092–3108.
[13] Y. Zheng, L.H. Lin, B. Wang, X.C. Wang, Angew. Chem. Int. Ed. 54 (2015) 12868–12884.
[14] J.M. Cai, Y.M. Zhu, D.S. Liu, M. Meng, Z.P. Hu, Z. Jiang, ACS Catal. 5 (2015) 1708–1716.
[15] G. Liu, P. Niu, C.H. Sun, S.C. Smith, Z.G. Chen, G.Q. Lu, H.M. Cheng, J. Am. Chem. Soc. 132 (2010) 11642–11648.
[16] G.G. Zhang, M.W. Zhang, X.X. Ye, X.Q. Qiu, S. Lin, X.C. Wang, Adv. Mater. 26 (2014) 805–809.
[17] Y.T. Gong, P.F. Zhang, X. Xu, Y. Li, H.R. Li, Y. Wang, J. Catal. 297 (2013) 272–280.
[18] X.C. Wang, X.F. Chen, A. Thomas, X.Z. Fu, M. Antonietti, Adv. Mater. 21 (2009) 1609–1612.
[19] S.F. Chen, Y.F. Hu, S.G. Meng, X.L. Fu, Appl. Catal. B: Environ. 150 (2014) 564–573.
[20] M.J. Muñoz-Batista, M. Fernández-García, A. Kubacka, Appl. Catal. B: Environ. 164 (2015) 261–270.
[21] X.J. Bai, C.P. Sun, S.L. Wu, Y.F. Zhu, J. Mater. Chem. A 3 (2015) 2741–2747.
[22] D.S. Wang, H.T. Sun, Q.Z. Luo, X.L. Yang, R. Yin, Appl. Catal. B: Environ. 156 (2014) 323–330.
[23] X.J. Bai, J. Li, C.B. Cao, S. Hussain, Mater. Lett. 65 (2011) 1101–1104.
[24] X.H. Li, X.C. Wang, M. Antonietti, Chem. Sci. 3 (2012) 2170–2174.
[25] Z.Y. Wang, W. Guan, Y.J. Sun, F. Dong, Y. Zhou, W.K. Ho, Nanoscale 7 (2015) 2471–2479.
[26] X.C. Wang, K. Maeda, X.F. Chen, K. Takanabe, K. Domen, Y.D. Hou, X.Z. Fu, M. Antonietti, J. Am. Chem. Soc. 131 (2009) 1680–1681.
[27] W.Z. Shen, L.W. Ren, H. Zhou, S.C. Zhang, W.B. Fan, J. Mater. Chem. 21 (2011) 3890–3894.
[28] Y.J. Cui, J.S. Zhang, G.G. Zhang, J.H. Huang, P. Liu, M. Antonietti, X.C. Wang, J. Mater. Chem. 21 (2011) 13032–13039.
[29] J.D. Xiao, Y.B. Xie, H.B. Cao, Chemosphere 121 (2015) 1–17.
[30] F.J. Beltrán, A. Aguinaco, A. Rey, J.F. García-Araya, Ind. Eng. Chem. Res. 51 (2012) 4533–4544.
[31] M. Fathinia, A. Khataee, Appl. Catal. A: Gen. 491 (2015) 136–154.
[32] G. Márquez, E.M. Rodríguez, F.J. Beltrán, P.M. Álvarez, Chemosphere 113 (2014) 71–78.
[33] G.Z. Liao, D.Y. Zhu, L.L. Li, B.Y. Lan, J. Hazard. Mater. 280 (2014) 531–535.
[34] J.D. Xiao, Y.B. Xie, H.B. Cao, Y.Q. Wang, Z.J. Zhao, Catal. Commun. 66 (2015) 10–14.
[35] J.D. Xiao, Y.B. Xie, F. Nawaz, S. Jin, F. Duan, M.J. Li, H.B. Cao, Appl. Catal. B: Environ. 181 (2016) 420–428.
[36] J. Beltran-Heredia, J. Torregrosa, J.R. Dominguez, J.A. Peres, Chemosphere 42 (2001) 351–359.
[37] J. Criquet, N.K.V. Leitner, Radiat. Phys. Chem. 106 (2015) 307–314.
[38] Z.Z. Lin, X.C. Wang, Angew. Chem. Int. Ed. 52 (2013) 1735–1738.
[39] F. Dong, Y.J. Sun, L.W. Wu, M. Fu, Z.B. Wu, Catal. Sci. Technol. 2 (2012) 1332–1335.
[40] B.H. Long, J.L. Lin, X.C. Wang, J. Mater. Chem. A 2 (2014) 2942–2951.
[41] J.S. Zhang, F.S. Guo, X.C. Wang, Adv. Funct. Mater. 23 (2013) 3008–3014.
[42] Z.F. Huang, J.J. Zou, L. Pan, S.B. Wang, X.W. Zhang, L. Wang, Appl. Catal. B: Environ. 147 (2014) 167–174.
[43] H.H. Ji, F. Chang, X.F. Hu, W. Qin, J.W. Shen, Chem. Eng. J. 218 (2013) 183–190.